

# Phase separation and toughening of SiC–AlN solid-solution ceramics

MASASHI MIURA, TOSHINOBU YOGO, SHIN-ICHI HIRANO

*Department of Applied Chemistry, School of Engineering, Nagoya University, Furo-cho, Chikusa-ku, Nagoya 464-01, Japan*

SiC–AlN solid-solution ceramics were prepared by pressureless sintering using  $\text{Al}_2\text{O}_3$  and  $\text{Y}_2\text{O}_3$  as the sintering additives. The resulting ceramics were subjected to annealing treatments over a range of temperatures from 1400 °C to 1800 °C in the spinodal region. The fracture toughness of the annealed ceramics was examined, by the indentation method, in relation to the annealing temperature and annealing time. X-ray diffraction profiles revealed that phase separation occurred during annealing. In ceramics containing 50 mol % SiC annealed at 1800 °C, the morphology of the phase separation is the characteristic modulated stratiform structure. Energy-dispersive X-ray spectroscopy (EDS) showed that the structure consisted of alternations of silicon-rich and aluminium-rich composition. The fracture toughness of the annealed ceramics increased compared to the as-sintered solid-solution ceramics. The phase separation is expected to contribute to the toughening of ceramics with nanometre-scale texture.

## 1. Introduction

Silicon carbide is expected to be a structural material which can be employed at higher temperature ranges where silicon nitride is no longer useful. However, its low fracture toughness has to be overcome before promoting the application of silicon carbide ceramics as engineering components. The toughening of silicon carbide ceramics is a great challenge. One approach for reinforcement is the combination of more than two different materials, such as fibres, whiskers, platelets and particles [1, 2, 3]. However, the strength of these composites was reduced by the residual defects in the sintered body. So far, *in situ* fabrication of ceramic composites and controlling the microstructure during sintering or annealing are expected to solve simultaneously the problems encountered in silicon-carbide ceramics. One example of *in-situ* toughening has been confirmed in silicon-nitride ceramics. The  $\beta$ -grains of silicon nitride are elongated in the silicon-nitride matrix during sintering by choosing the appropriate sintering additives [4, 5]. For the toughening of silicon-carbide ceramics, this work paid attention to the existence of a miscibility gap in the SiC–AlN system [6]. Rafaniello *et al.* [7] showed that a SiC–AlN solid solution decomposes into two isostructural 2H phases below about 2200 °C. However, they did not evaluate the contributions of the modulated structure, produced by annealing, to the fracture toughness.

This work focuses on the *in-situ* processing of SiC–AlN nanometer-level composites by annealing solid-solution ceramics, and also on the evaluation of the toughening of SiC-based ceramics. The annealing of solid-solution ceramics in the spinodal region was found to result in a nano-composite composed of a

SiC-rich domain and a AlN-rich domain, leading to improvement of the mechanical properties.

## 2. Experimental procedure

### 2.1. Raw materials

To obtain dense and single phase SiC–AlN solid-solution ceramics by pressureless sintering,  $\text{Y}_2\text{O}_3$  and  $\text{Al}_2\text{O}_3$  were selected as sintering additives [8]. The properties of  $\beta$ -SiC, AlN,  $\alpha$ - $\text{Al}_2\text{O}_3$  and  $\text{Y}_2\text{O}_3$  powders used in this experiment are listed in Table I.

### 2.2. Preparation of the green compacts

Appropriate amounts of the raw powder materials were mixed with isopropyl alcohol in a plastic ball mill for 20 h. The molar ratios of SiC to AlN, the amounts of additives, and their abbreviations are shown in Table II. After drying the slurry at 220 °C, the mixture powders were sieved through a 60-mesh screen. The powder was die pressed under 50 MPa and then isostatically pressed under 290 MPa.

### 2.3. Preparation of the SiC–AlN solid solution

The compacts were placed in a carbon crucible and packed in a powder bed of the same composition, and placed in the hot zone of the furnace. The compacts were fired at a heating rate of 20 °C  $\text{min}^{-1}$  to 1100 °C, followed by heating at 10 °C  $\text{min}^{-1}$  to 2000 °C and then 5 °C  $\text{min}^{-1}$  to 2200 °C. The retaining time at the maximum temperature was 8 h. All these sintering processes were carried out in a flow of Ar at ambient pressure.

**2.4. Annealing of the SiC–AlN solid solution**  
Annealing was undertaken over a temperature range between 1400 and 1800 °C in an Ar atmosphere for periods of up to 28 h. The compositions for these annealing treatments are shown in Table II.

### 2.5. Characterization

Characterization was performed on the interior of the specimens. The sintered and annealed SiC–AlN ceramics were ground to remove the surface layer finishing with a 1 µm diamond paste prior to the evaluation of the properties.

#### 2.5.1. Density

The density of the sintered ceramics was measured by the Archimedes method using distilled water. The theoretical density of each composition was calculated based upon the densities and the molar fractions of the constituents.

#### 2.5.2. Crystal phases and lattice constants

The crystal phases were characterized by X-ray diffraction (XRD) using  $\text{CuK}_\alpha$  radiation at 40 kV and 30 mA. Silicon was used as an internal standard for accurate determination of the lattice constant.

#### 2.5.3. Fracture toughness and hardness

The indentation-fracture-test method was used with a 100 N load on the finished surfaces of the specimens for the measurements of fracture toughness and hardness.

#### 2.5.4. Microstructural observation

The microstructure of the annealed ceramics was examined by transmission electron microscopy (TEM). Energy-dispersive X-ray spectrometry (EDS) was used to analyse quantitatively the composition change within the matrix. For optical microscopy observation, the polished samples were etched with Murakami's solution.

TABLE I Properties of raw powders\*

$\beta$ -SiC	Beta Random, Ividen Company Free $\text{SiO}_2$ (0.39 wt %) Free C (0.64 wt %) Al (0.02 wt %) Fe (0.03 wt %) Average particle size = 0.27 µm Specific surface area = 20.4 m <sup>2</sup> g <sup>-1</sup>
AlN	Type F, Tokuyama Soda Company O (0.82 wt %) C (440 p.p.m.) Ca (34 p.p.m.) Si (10 p.p.m.) Fe (10 p.p.m.) Specific surface area = 3.3 m <sup>2</sup> g <sup>-1</sup>
$\alpha$ -Al <sub>2</sub> O <sub>3</sub>	AKP-30, Sumitomo Chemical Company Purity > 99.99% Si (9 p.p.m.) Na (2 p.p.m.) Mg (3 p.p.m.) Fe (9 p.p.m.) Average particle size = 0.40 µm Specific surface area = 7.4 m <sup>2</sup> g <sup>-1</sup>
Y <sub>2</sub> O <sub>3</sub>	Mitsubishi Chemical Company Purity (>99.9%) Fe (6.7 p.p.m.) Ca (<0.5 p.p.m.)

\*Data obtained from the manufactures.

## 3. Results and Discussion

### 3.1. Pressureless sintering of SiC–AlN solid solution

#### 3.1.1. Sintering additives

Table III shows the relative densities of the compacts sintered at 2200 °C for 8 h in Ar at ambient pressure. The specimens containing Y<sub>2</sub>O<sub>3</sub> could be densified at a temperature as low as 2000 °C and for a sintering time up to 8 h. The densification was accelerated by the formation of a liquid phase during the sintering by the addition of Y<sub>2</sub>O<sub>3</sub>. Fig. 1 shows typical XRD patterns of one of the ceramics sintered at a lower temperature (the composition is the same as the SA50A3Y ceramic sintered at 2100 °C for 4 h). The crystalline phases consist of two main phases; one is a SiC-rich solid-solution phase and the other is an AlN-rich solid-solution phase. The formation of SiC–AlN solid solution could be performed completely under sintering temperatures in the range 2150–2200 °C.

The addition of 1 mol % Y<sub>2</sub>O<sub>3</sub> was found to be too much additive, because the SA50Y1 specimen was very porous due to the excess formation of a liquid phase in quantity during the sintering at 2200 °C. In spite of the addition of 3 mol % Al<sub>2</sub>O<sub>3</sub>, the SA50A3 specimen did not densify. Specimens with the other compositions had a relative density above 97%. From

TABLE II Nominal compositions of powder mixtures

Sample name	Composition (mol %)					Annealing Temp. (°C)
	SiC/AlN ratio	SiC	AlN	Al <sub>2</sub> O <sub>3</sub>	Y <sub>2</sub> O <sub>3</sub>	
SA50Y	50/50	49.75	49.75		0.5	
SA50Y1	50/50	49.50	49.50		1.0	
SA50A3	50/50	48.50	48.50	3.0		
SA50A1Y	50/50	49.25	49.25	1.0	0.5	1400, 1600, 1800
SA50A3Y	50/50	48.25	48.25	3.0	0.5	1600, 1800
SA70A1Y	70/30	68.95	29.55	1.0	0.5	1400, 1600, 1800

TABLE III Effect of sintering additives on the sinterability of the SiC–AlN system

Sample name	Relative density (%)	Comments
SA50Y	97.2	
SA50Y1		Porous
SA50A3		Not sintered
SA50A1Y	97.5	
SA50A3Y	96.7	
SA70A1Y	97.5	

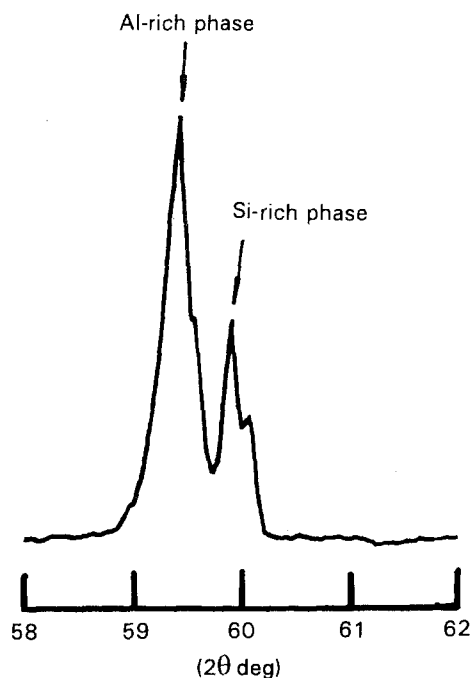


Figure 1 XRD pattern of the SiC–AlN ceramic sintered at 2100 °C for 4 h. (SiC/AlN = 50/50, Al<sub>2</sub>O<sub>3</sub> (3.0 mol %), Y<sub>2</sub>O<sub>3</sub> (0.5 mol %)).

these results, a 0.5 mol % Y<sub>2</sub>O<sub>3</sub>–1.0 mol % Al<sub>2</sub>O<sub>3</sub> system (specimen SA50A1Y and SA70A1Y), and a 0.5 mol % Y<sub>2</sub>O<sub>3</sub>–3.0 mol % Al<sub>2</sub>O<sub>3</sub> system (specimen SA50A3Y) were selected as sintering additives for the further annealing experiments.

### 3.1.2. Crystalline phases

The XRD patterns on SA50A1Y and SA70A1Y ceramics sintered at 2200 °C for 8 h are shown in Fig. 2. The major crystalline phase in these samples was a SiC–AlN(2H) solid solution and the minor phase was an unknown phase which is expected to be derived from the sintering additives.

Table IV summarizes the lattice constants of the SA50A1Y and SA70A1Y ceramics. The lattice constants of both ceramics are in good agreement with the graph of lattice constants of SiC–AlN solid-solutions against composition by Zangvil and Ruh [9].

## 3.2. Annealing of the SiC–AlN solid solution in the phase-separation region

The SiC–AlN solid-solution ceramics (SA50A1Y, SA50A3Y and SA70A1Y) were annealed at 1400 °C, 1600 °C or 1800 °C for periods up to 28 h.

TABLE IV Lattice constants of SiC–AlN solid solutions

Sample name	SiC/AlN ratio	Lattice constant (nm)	
		<i>a</i>	<i>c</i>
SA50A1Y	50/50	0.3102 (0.3100 <sup>a</sup> )	0.5020 (0.5018 <sup>a</sup> )
SA70A1Y	70/30	0.3092 (0.3092 <sup>a</sup> )	0.5038 (0.5033 <sup>a</sup> )

<sup>a</sup> From the graph of Zangvil and Ruh [9]

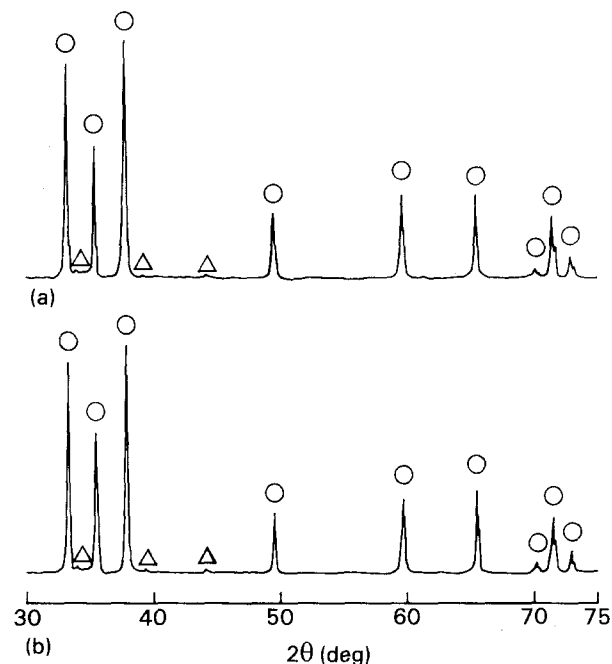


Figure 2 XRD patterns of SiC–AlN solid-solution ceramics sintered at 2200 °C for 8 h: (○) SiC–AlN solid solution, and (△) unknown. (a) SA50A1Y (SiC/AlN = 50/50, Al<sub>2</sub>O<sub>3</sub> = 1 mol %, Y<sub>2</sub>O<sub>3</sub> = 0.5 mol %), and (b) SA70A1Y (SiC/AlN = 70/30, Al<sub>2</sub>O<sub>3</sub> = 1 mol %, Y<sub>2</sub>O<sub>3</sub> = 0.5 mol %).

### 3.2.1. Crystal-phase changes by annealing

Fig. 3 shows the crystalline-phase changes of the ceramics (SA70A1Y, SA50A3Y) by annealing at 1800 °C. The (1 1 0) peak of both ceramics, exhibits splitting, indicating that phase separation does take place. This phase separation was presumed to be of spinodal or binodal decomposition, considering the peak splitting behaviour [10, 11].

### 3.2.2. Microstructural observation by TEM and EDS

Fig. 4 shows a TEM image of the SA50A3Y ceramic annealed at 1800 °C for 22 h. The specimen was furnace cooled and not quenched after sintering or annealing. The microstructure of the annealed specimens shows stratiform modulations with preferred directionality. Such a microstructure has often been observed in spinodally-decomposed materials [10, 11]. Zangvil and Ruh [6] showed the existence of a miscibility gap below 1950 °C in SiC–AlN systems. Also, in the study of Kuo and Virkar [12], hot-pressed SiC–AlN ceramics decomposed by annealing treatment had cellular precipitation in the crystal grains.

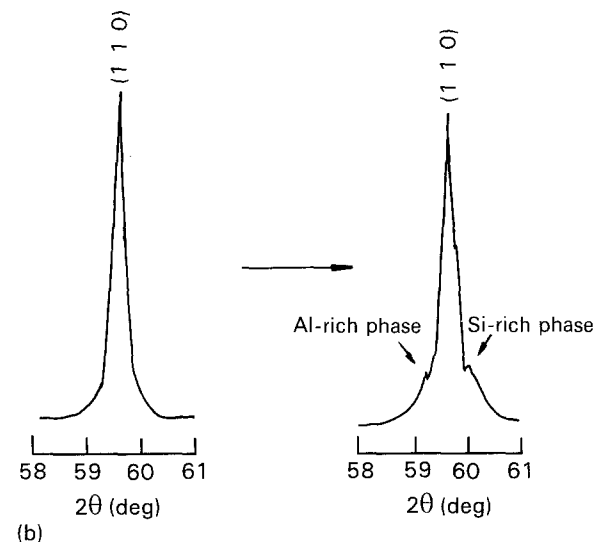
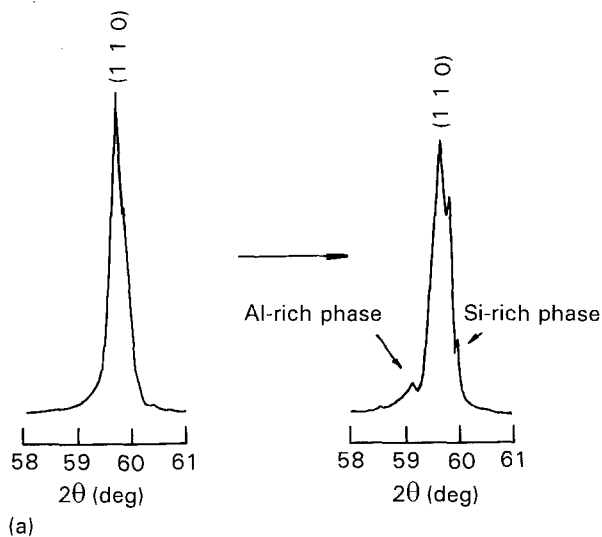


Figure 3 Crystal-phase changes of SiC–AlN ceramics: (a) SA70A1Y ceramics annealed at 1800 °C for 16 h, and (b) SA50A3Y ceramics annealed at 1800 °C for 22 h.

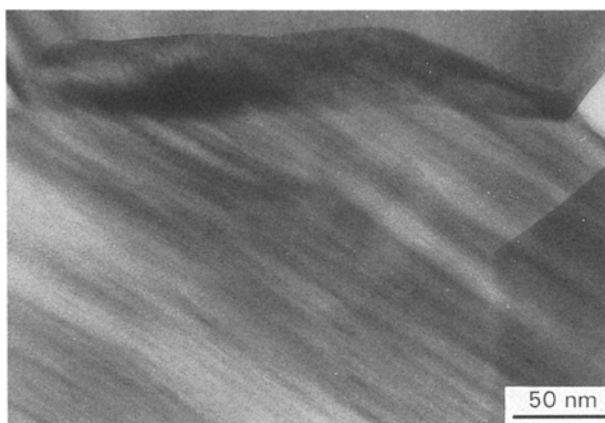


Figure 4 TEM of SA50A3Y ceramics annealed at 1800 °C for 22 h.

The difference in the microstructure between hot-pressed and pressureless sintered ceramics may be attributed to the effects of the sintering additives, sintering conditions, annealing conditions and so on.

The results of microanalysis by EDS are shown in Fig. 5. The dark area has a relatively higher area of Al

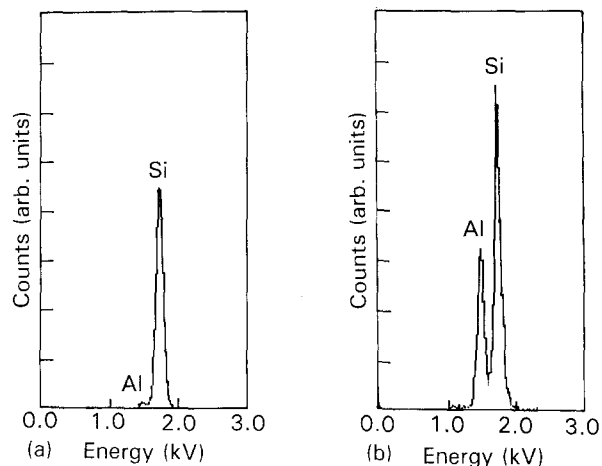


Figure 5 EDS analysis of SA50A3Y ceramics annealed at 1800 °C for 22 h: (a) bright area, and (b) dark area.

content than the bright area. This indicates that the stratiform structure is produced by phase separation such as spinodal decomposition. Whereas the hot-pressed SiC–AlN solid solution requires longer annealing times for phase separation [12], ceramics sintered under the pressureless condition decompose in a shorter period (less than 22 h annealing time). The difference between the hot-pressed and pressureless sintered ceramics reflects whether a sintering additive is used or not. Yuan and Virkar [11] and Hirano *et al.* [13] also considered the role of aliovalent dopants on the kinetics of spinodal decomposition. According to their work, Al<sub>2</sub>O<sub>3</sub> doping enhances the kinetics of the decomposition of TiO<sub>2</sub>–SnO<sub>2</sub> systems. Y or/and O are also expected to affect the kinetics of spinodal decomposition in SiC–AlN systems.

### 3.2.3. Fracture toughness and hardness

Fig. 6 and Fig. 7 show the relations between the fracture toughness of the SA50A1Y and SA70A1Y ceramics and the annealing time and temperature. The low initial  $K_{Ic}$  might be due to the relatively coarse matrix grains. The fracture toughness of both specimens increases with annealing time at all annealing temperatures in the spinodal region of each SiC–AlN system. The temperature dependences of the improvement of the fracture toughness are different. In the SA50A1Y ceramics, the behaviour of the increase in fracture toughness is similar for annealing at 1600 °C and 1800 °C. This suggests that the phase separation behaviour and the modulated structure developed in the matrix at 1600 °C are similar to those at 1800 °C. At 1400 °C, the fracture toughness of the specimen increases more slowly with annealing time than at 1600 °C and above. In the SA70A1Y ceramics, however, the fracture toughness of the specimen annealed at 1800 °C increases more slowly than those at 1600 °C and 1400 °C. According to the phase diagram of the SiC–AlN system suggested by Zangvil and Ruh [6], the miscibility gap in these compositions (SiC/AlN = 70/30, 50/50) exists at around 1850 °C, which implies that the spinodal line lies in a lower temperature region below 1850 °C. Assuming that the top of the

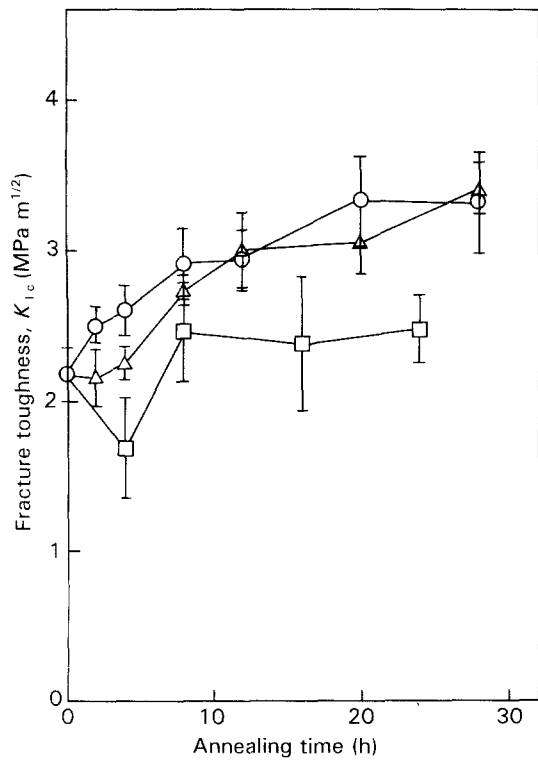


Figure 6 Fracture toughness changes of SA50A1Y ceramics for various annealing temperatures: (□) 1400°C, (△) 1600°C, and (○) 1800°C. (SiC/AlN = 50/50, Al<sub>2</sub>O<sub>3</sub> = 1.0 mol %, Y<sub>2</sub>O<sub>3</sub> = 0.5 mol %).

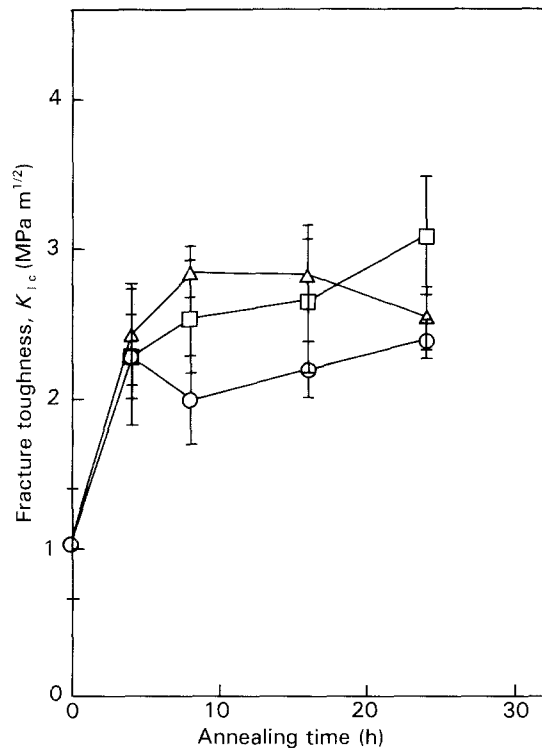


Figure 7 Fracture toughness changes of SA70A1Y ceramics for various annealing temperatures: (□) 1400°C, (△) 1600°C, and (○) 1800°C. (SiC/AlN = 70/30, Al<sub>2</sub>O<sub>3</sub> = 1.0 mol %, Y<sub>2</sub>O<sub>3</sub> = 0.5 mol %).

spinodal dome exists around the composition of 50 mol % SiC, the different behaviour in the change of fracture toughness with the annealing temperature can be explained as follows. At all annealing temper-

atures, the composition of the SA50A1Y ceramic is located inside the spinodal region. Therefore, the difference of the toughness change depends on the rate of the decomposition. In contrast, in the composition of SA70A1Y, the spinodal dome is located in a lower temperature region than in a SA50A1Y composition. The fact that the fracture toughness of the ceramics annealed at 1800°C increases more slowly than the other temperatures reflects that the spinodal decomposition region exists between 1600°C and 1800°C at this composition.

Fig. 8 shows the fracture toughness changes of the SA50A3Y ceramics. The SiC/AlN ratio of SA50A3Y is the same as that of SA50A1Y, except the amount of Al<sub>2</sub>O<sub>3</sub> is different. The initial increase of the fracture toughness of SA50A3Y ceramics is more rapid than in SA50A1Y. The different amount of Al<sub>2</sub>O<sub>3</sub> is considered to affect the total concentration of oxygen in the specimens. The results also suggest that the solution of oxygen in the SiC-AlN system influences the rate of the phase separation.

The changes of the hardness by annealing are shown in Figs 9–11. The hardness of each ceramic increases gradually with annealing. An age-hardening effect was observed in the SiC-AlN system (as in alloys). The effect might also be related to the microstructural development by spinodal decomposition, although the mechanism has not been confirmed yet.

### 3.2.4. Observation of crack propagation by optical microscopy

Figs 12 and 13 show the propagation of cracks introduced by the indentation method on the surfaces of

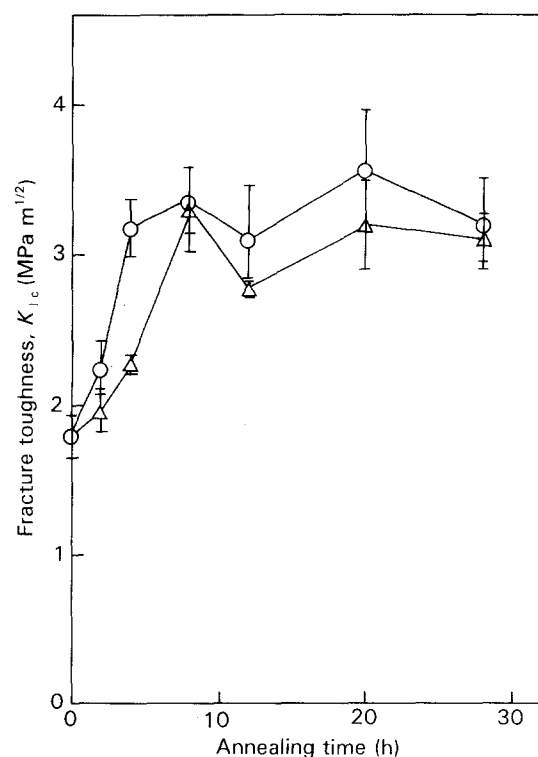


Figure 8 Fracture toughness changes of SA50A3Y ceramics for annealing temperatures: (△) 1600°C, and (○) 1800°C. (SiC/AlN = 50/50, Al<sub>2</sub>O<sub>3</sub> = 3 mol %, Y<sub>2</sub>O<sub>3</sub> = 0.5 mol %).

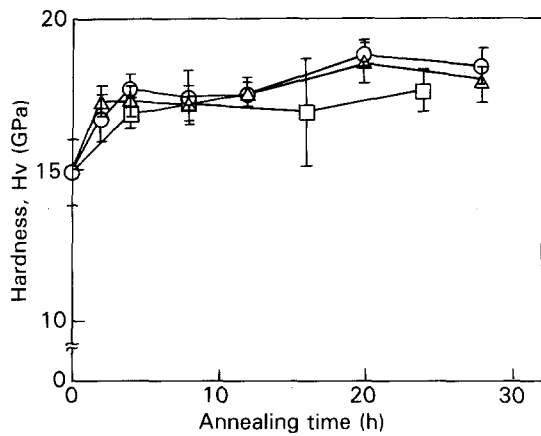


Figure 9 Hardness changes of SA50A1Y ceramics for annealing temperatures: (□) 1400°C, (△) 1600°C, and (○) 1800°C. (SiC/AlN = 50/50, Al<sub>2</sub>O<sub>3</sub> = 1.0 mol %, Y<sub>2</sub>O<sub>3</sub> = 0.5 mol %).

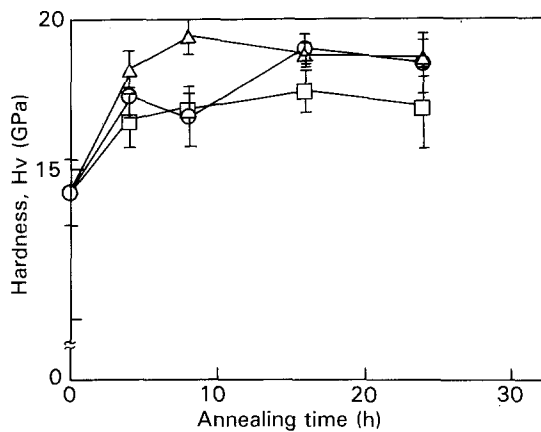


Figure 10 Hardness changes of SA70A1Y ceramics for annealing temperatures: (□) 1400°C, (△) 1600°C, and (○) 1800°C. (SiC/AlN = 70/50, Al<sub>2</sub>O<sub>3</sub> = 1.0 mol %, Y<sub>2</sub>O<sub>3</sub> = 0.5 mol %).

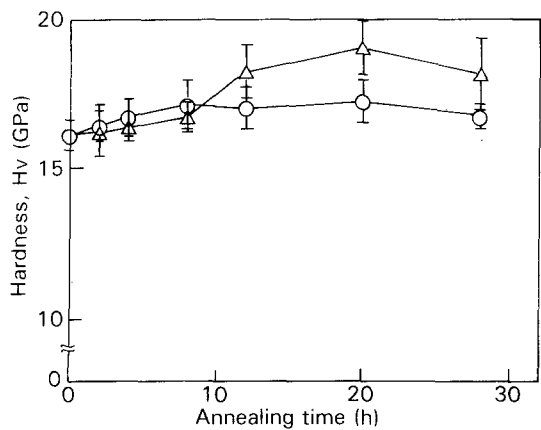


Figure 11 Hardness changes of SA50A3Y ceramics for annealing temperatures: (△) 1600°C, and (○) 1800°C. (SiC/AlN = 50/50, Al<sub>2</sub>O<sub>3</sub> = 3 mol %, Y<sub>2</sub>O<sub>3</sub> = 0.5 mol %).

the as-sintered and as-annealed specimens. Both specimens have similar polycrystalline structures. The indentation crack propagates through the grains in both specimens. This phenomenon is different from the result by Lee and Wei [14]. They explained that the elongated SiC-rich grains resulted in crack-deflection, leading to the toughening of the ceramics. In the case

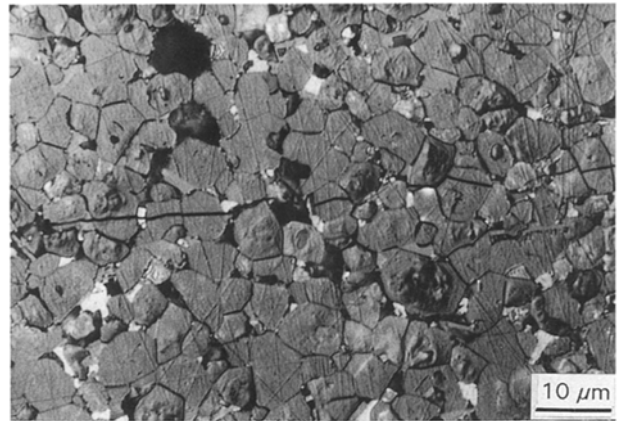


Figure 12 Photograph of propagation of crack. (SA50A3Y, as-sintered ceramic).

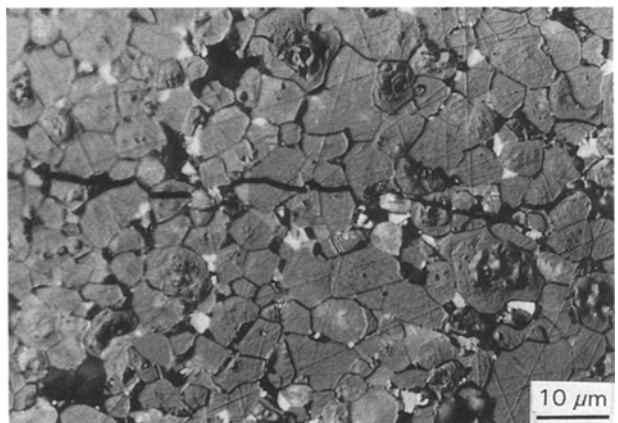


Figure 13 Photograph of propagation of crack. (SA50A3Y, as-annealed ceramic; 1800°C, 28 h).

of the annealed SiC–AlN ceramics prepared in this work, the grains are granular after annealing and crack-deflection at the grain boundary was not observed. The increase of fracture toughness of the present SiC–AlN annealed ceramics can be explained by absorption of the fracture energy by modulated grains when the cracks propagate through the intragrain. The interface effect resulting from the residual stress due to the differences in the thermal-expansion coefficient and the elastic modulus of the two phases may be expected to cause crack shielding and/or crack deflection and increase the fracture toughness of the ceramics with the layered microstructure.

#### 4. Conclusion

SiC–AlN solid-solution ceramics were prepared by pressureless sintering at 2200°C for 8 h using Al<sub>2</sub>O<sub>3</sub> and Y<sub>2</sub>O<sub>3</sub> as the sintering additives. Phase separation did occur by annealing the solid solutions (SiC/AlN = 70/30 and 50/50) in the phase-separation region and the fracture toughness could be increased by varying the annealing parameters (time and temperature). This phase separation is recognized as spinodal decomposition by the characteristic features detected

by XRD, TEM and EDS. The modulated structure of the crystal grains contributes to the toughening of the SiC-based ceramics. Further work is underway to evaluate the toughening mechanism.

### Acknowledgements

We thank Mr Suzuki of JFCC (Japan Fine Ceramics Center) for helping with the TEM and EDS measurements.

### References

1. F. ABBE and J. CHERMANT, *J. Amer. Ceram. Soc.* **73** (1990) 2573.
2. R. VELTRI, D. CONDIT and F. GALASSO, *J. Amer. Ceram. Soc.* **72** (1989) 478.
3. G. C. WEI and P. F. BECHER, *J. Amer. Ceram. Soc.* **67** (1984) 571.
4. A. G. EVANS, *J. Amer. Ceram. Soc.* **73** (1990) 187.
5. G. HIMSOLT, H. KNOCH, H. HUBNER and F. W. KLEINLEIN, *J. Amer. Ceram. Soc.* **62** (1979) 29.
6. A. ZANGVIL and R. RUH, *J. Amer. Ceram. Soc.* **71** (1988) 884.
7. J. W. RAFANIELLO, M. R. PLICHTA and A. V. VIRKAR, *J. Amer. Ceram. Soc.* **66** (1983) 272.
8. W. WEI and R. LEE, *J. Mater. Sci.* **26** (1991) 2930.
9. A. ZANGVIL and R. RUH, *J. Mater. Sci. Lett.* **3** (1984) 249.
10. M. W. PARK, T. E. MITCHELL and A. H. HEUER, *J. Mater. Sci.* **11** (1976) 1227.
11. T. C. YUAN and A. V. VIRKAR, *J. Amer. Ceram. Soc.* **71** (1988) 12.
12. S. KUO and A. V. VIRKAR, *J. Amer. Ceram. Soc.* **73** (1990) 2640.
13. S. HIRANO, T. YOGO, K. KIKUTA, S. ARAKAWA, Y. SEKI and M. KAWAMOTO, in "Ceramic transactions", Vol. 22 (American Ceramic Society, Westerville, OH, 1991) p. 727.
14. R. LEE and W. WEI, *Ceram. Engng. Sci. Proc.* **11** (1990) 1094.

*Received 26 February  
and accepted 10 December 1992*